Screening of coformers for quercetin cocrystals through mechanochemical methods

Fayene Zeferino Ribeiro de Souza[1] , Amanda Cosmo de Almeida[1] , Patrícia Osorio Ferreira[1] , Richard Perosa Fernandes[2] , Flávio Junior Caires[1+]

1. São Paulo State University, School of Science, Bauru, Brazil.
2. São Paulo State University, Institute of Chemistry, Araraquara, Brazil.

+Corresponding author: Flávio Junior Caires, Phone: +55 14 3103-9830, Email address: flavio.caires@unesp.br

ABSTRACT: Quercetin (QUE) is a nutraceutical compound that exhibits pharmacological properties such as antioxidant, cardioprotective, anti-ulcer, and anti-inflammatory effects. Although QUE is well-known for its benefits, its efficacy is limited due to low solubility. Thus, cocrystallization acts as an interesting approach to improve the solubility—among other properties—of this compound. In this work, cocrystallization screening was applied through neat grinding (NG) and liquid-assisted grinding (LAG), in which QUE and four cocrystal formers (benzamide, picolinamide, isonicotinamide,

and pyrazinoic acid) were tested. The precursors and QUE-coformer systems were characterized using thermoanalytical techniques (TG-DTA), X-ray powder diffraction (XRPD), and Fourier transform infrared (FTIR) spectroscopy. The results showed the formation of QUE cocrystals with picolinamide and isonicotinamide coformers in a 1:1 stoichiometric ratio. Furthermore, although coformers are isomers, spectroscopic and thermal data suggest that the supramolecular synthons involved in cocrystallization are different.
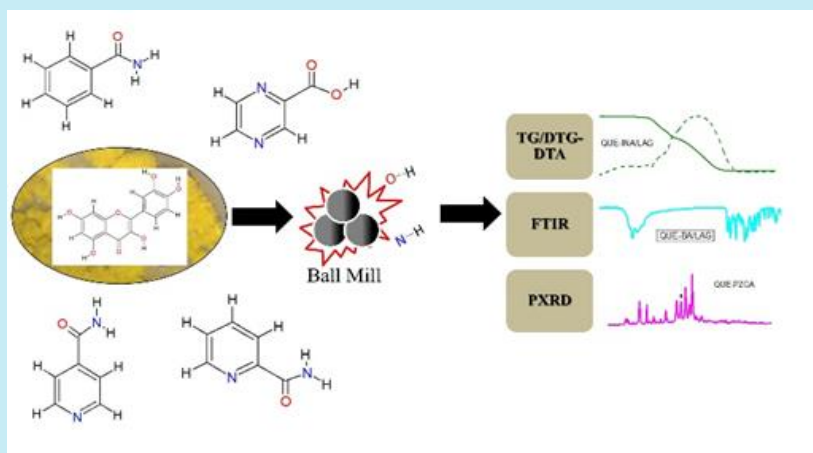
1. Introduction

Nutraceuticals are chemical compounds present in functional foods with medicinal benefits, which aid in the prevention and treatment of diseases. Among them are vast natural products such as phenolic acids, coumarins, vitamins, and compounds from the flavonoid class, including quercetin (QUE) (Madaan *et al.*, 2016; Sinha *et al.*, 2015; Thakuria and Sarma, 2018).

Quercetin is a polyphenol flavonoid commonly found in many types of fruits, vegetables, and teas, being more abundant in onions (Tang *et al.*, 2016). This important flavonol shows biological properties, including antioxidant, cardioprotective, anti-ulcer, and anti-inflammatory effects (Madaan *et al.*, 2016; Varzakas *et al.*, 2016; Vasisht *et al.*, 2016). Although QUE is well-known for its therapeutic bioactivity, this substance is classified as class II in Biopharmaceutical Classification System (BCS), with low aqueous solubility and high permeability, which limits its efficacy (Sinha *et al.*, 2015). Given this context, approaches such as cocrystallization have been employed aiming at the improvement of physical-chemical properties, like solubility, stability, bioavailability, and others, without changing therapeutic properties (Aakeröy *et al.*, 2009; Madaan *et al.*, 2016; Su *et al.*, 2015).

Cocrystal is a crystalline material formed through non-covalent intermolecular interactions, as Van der Waals forces, hydrogen bonding, π-π interactions, halogen bonding, and others without proton transfer. In terms of applicability in the pharmaceutical field, the cocrystal could be designed by an active pharmaceutical ingredient (API) and a nontoxic and safe substance for consumption, known as coformer (Panzade *et al.*, 2017; Yadav *et al.*, 2009).

The QUE molecule can form intermolecular interactions through its five hydroxyl groups that provide several different conformations, making it possible to establish supramolecular synthons (Dubey and Desiraju, 2015). Thus, the coformers of benzamide (BA), picolinamide (PA), isonicotinamide (INA), and pyrazinoic acid (PZCA) were selected based on safety and the possibility of their functional groups interacting with quercetin. Although the INA coformer has been reported to form a QUE–INA cocrystal synthesized via the slurry method (Smith *et al.*, 2011), here the preparation of this cocrystal was investigated through grinding methods. The structural formulas of quercetin and coformers are shown in Fig. 1.
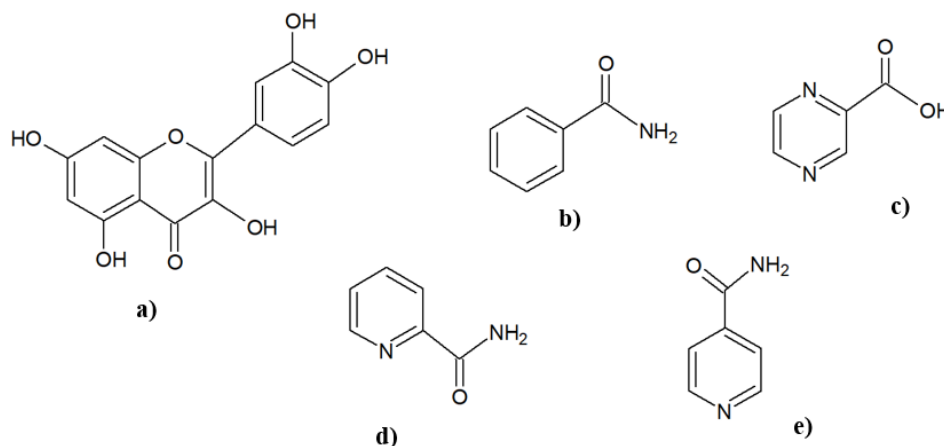

Figure 1.Structural formula of quercetin (**a**) and the coformers benzamide (**b**), pyrazinoic acid (**c**), picolinamide (**d**), isonicotinamide (**e**).

Many APIs that have problems related to their physicochemical properties highlight the importance of the cocrystals approach by the pharmaceutical industry. Moreover, the new crystal form resulting from the interaction between an API and another molecule could be patented, as in the already marketed Entresto, Steglatro, Depakote, Lexapro, and others (Karagianni *et al.*, 2018; Karimi-Jafari *et al.*, 2018; Kavanagh *et al.*, 2019; Patel *et al.*, 2019; Qiao *et al.*, 2011; Rajput *et al.*, 2013; Sathisaran and Dalvi, 2018; Yousef and Vangala, 2019).

Given the context, this work describes cocrystal screening for QUE employing four coformers by two different mechanochemical methods, neat grinding (NG) and liquid-assisted grinding (LAG), performing spectroscopic and diffractometric characterization, and thermoanalytical studies.

2. Experimental part

2.1 Materials

Benzamide, PA, INA, and PZCA (all with >99% purity) were purchased from Sigma Aldrich, QUE (95.0% dry extract) was purchased from a local drugstore. The liquid used during the LAG method was ethanol (99.5% purity), purchased from Dinâmica. All reactants were used without further purification.

2.2 Methods

The mechanochemical synthesis was performed using two solid-state based methods, LAG and NG grindings were performed in a ball mill (Retsch, MM 400 model) using 10 mL stainless steel jars and 7 mm stainless steel balls, under a grinding frequency of 30 Hz for 30 min. The total mass of the milled sample was 500 mg in the molar ratio of 1:1 between the drug and each coformer. The amount of liquid (ethanol) added in the LAG synthesis was 0.25 μL mg^{-1} ratio (volume/total sample mass), based on studies by Friščić et al. (2009).

Simultaneous thermogravimetry-differential thermal analysis (TG-DTA) curves were obtained on a thermogravimetric analyzer (NETZCH, STA449 F3). The TG-DTA analyses, in the range of 30 to 800 °C, were performed with a heating rate of 10 °C min^{-1}, using an α-Al$_2$O$_3$ (70 μL) crucible under dynamic air atmosphere with a flow rate of 50 mL min^{-1}. The sample mass was approximately 5.0 mg.

X-ray powder diffraction (XRPD) analyzes were performed on the Rigaku MiniFlex 600 diffractometer, employing Cu Kα radiation (λ=1.54056 Å) in a 2θ range of 5° up to 50°, under continuous scan mode, with a rate of 4° min^{-1} and operating settings of 40 kV voltage and 15 mA current.

Infrared (FTIR) spectra were obtained using Nicolet iS10 FTIR spectrophotometer, Thermo Scientific, through an attenuated total reflectance method equipped with a germanium crystal, within a range of 675 to 4000 cm^{-1}, 32 scans per spectrum, 4 cm^{-1} of resolution.

To determine the solubility of the drug, the critical step is the quantification of the drug dissolved in the medium, since it is necessary to use a validated analytical method. It was already tried to quantify the drug using UV-visible spectrophotometric method, but the developed method did not show selectivity, the coformer interfered in the drug quantification. Furthermore, as reported by Ramešová et al. (2012),

QUE is unstable in aqueous solution, which would make its quantification difficult.

3. Results and discussion

3.1 Quercetin–isonicotinamide (1:1) system

3.1.1 X-ray powder diffraction and FTIR

The first system prepared in this work was an alternative approach to that reported by Smith et al.(2011). Their work showed the synthesis of a QUE–INA cocrystal prepared through slurry crystallization, a solution-based method dissolving the starting materials in 5–6 mL of methanol. Given the context, the cocrystal was prepared using mechanochemical synthesis as it is a greener, less solvent, faster and reproducible approach. Therefore, the XRPD diffractograms and FTIR spectra of QUE, INA, and the QUE–INA systems are shown in Fig. 2.
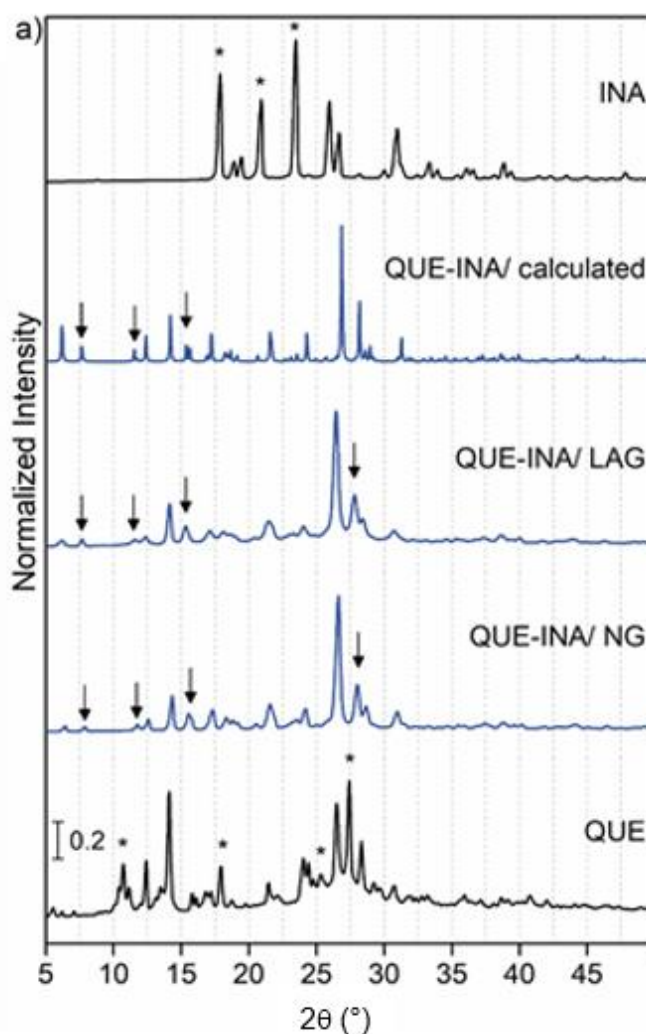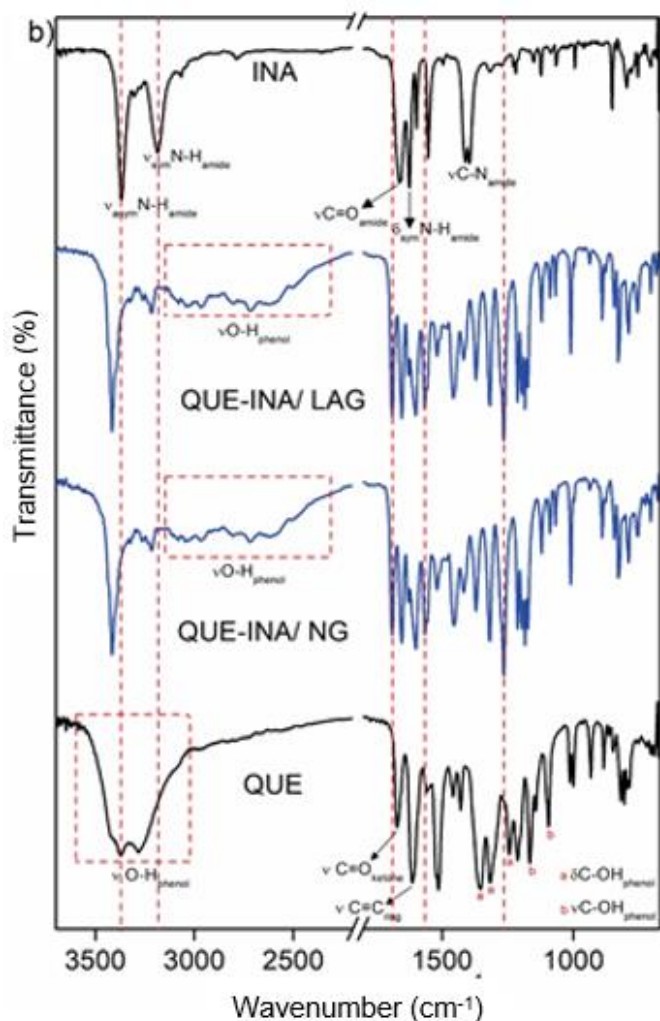
Figure 2. X-ray powder diffraction diffractograms **(a)** and FTIR spectra **(b)** of QUE, INA, and the QUE–INA (1:1) systems. (XRPD diffractogram calculated from the QUE–INA cocrystal was obtained using the Mercury program from the CIF file (CCDC Deposition Number: 1428198 of the crystalline structure reported by Smith *et al.* [2011])

The QUE–INA/NG and QUE–INA/LAG systems have the same diffraction pattern, with new diffraction peaks at 2θ equal to 7.9, 11.8, 15.5 and 28.0° and absence of diffraction peaks associated with the INA (17.9, 20.9 and 23.5°) and the QUE (5.5, 10.7, 17.9, 25.3 and 27.4°), confirming the formation of cocrystal. The diffractograms of these systems show the same diffraction pattern of the QUE–INA cocrystal reported in the literature that was obtained by the slurry method (Smith *et al.*, 2011), confirming that the synthesis method does not influence the crystalline phase formed and that the mechanochemical method is efficient in obtaining this cocrystal.

Regarding the FTIR data, the QUE spectrum shows the presence of strong broad bands with peaks at 3373 and 3281 cm^{-1} attributed to the O–H stretching vibrations (νO–H$_{phenol}$) of the phenol groups, a band at 1670 cm^{-1} attributed to the C=O stretching vibrations (νC=O$_{ketone}$) of the ketone carbonyl group, the bands at 1612 and 1212 cm^{-1} are attributed to the stretching vibrations of the aromatic ring (νC=C$_{ring}$) and the ether group (νC–O–C), respectively. The bands at 1355, 1316, and 1245 cm^{-1} are attributed to the C–OH bending vibrations of the phenol groups (δC–OH$_{phenol}$), and the bands at 1168 and 1097 cm^{-1} are attributed to the C–OH stretching vibrations of the phenol groups (νC–OH$_{phenol}$) (Nguyen and Jeong, 2018; Refat *et al.*, 2021).

The FTIR spectrum of INA shows bands at 3370 and 3185 cm^{-1} attributed to the asymmetric and symmetrical N–H stretching vibrations (ν_{asym}N–H$_{amide}$ *and* ν_{sym}N–H$_{amide}$), a band at 1661 cm^{-1} attributed to C=O stretching vibrations (νC=O$_{amide}$), a band at 1625 cm^{-1} attributed to N–H bending vibrations (δN–H$_{amide}$) and a band at 1403 cm^{-1} attributed to C–N stretching vibrations (νC–N$_{amide}$) (Yurdakul and Ataç, 2004).

The FTIR spectra of the QUE–INA/LAG and QUE–INA/NG systems are similar to each other and present significant changes in relation to the spectra of isolated precursors, suggesting the establishment of new supramolecular synthons in the solid-state. The ν_{asym}N–H and ν_{sym}N–H bands are shifted to higher absorption frequency values, and the intensity of ν_{sym}N–H band decreased significantly. Another significant change is associated with the νO–H$_{phenol}$ band, its intensity decreases, it became wider and shifted to a region of frequencies between 2316 and 3115 cm^{-1}, indicating the presence of hydrogen bonds of OH$_{(phenol)}$···N$_{(aromatic)}$ between the molecules (Rautenberg *et al.*, 2020; Ravikumar *et al.*, 2013), in accordance with the data of crystal structure reported by Smith *et al.* (2011). The bands associated with the vibrations of the carbonyl groups also undergo small displacements, the νC=O$_{ketone}$ of QUE was shifted to 1690 cm^{-1}, and that of the νC=O$_{amide}$ of INA was shifted to 1651 cm^{-1}. Finally, the bands associated with νC–N$_{amide}$, δC–OH$_{phenol}$, and νC–OH$_{phenol}$ shifted to higher absorption frequency values.

3.1.2 Simultaneous thermogravimetry-differential thermal analysis

The thermoanalytical curves of the QUE, INA and the QUE–INA/NG and QUE–INA/LAG systems are shown in Fig. 3. The TG curve of QUE shows that it is

thermally stable up to 290 °C and undergoes mass loss in at least three steps. The first step of mass loss between 30–120 °C (Δm_{QUE} = 4.96%), without a thermal event in the DTA curve, is associated with dehydration of the compound since QUE is marketed in its hydrated form (Ravikumar *et al.*, 2013). The second and third steps, corresponding to exothermic events in the DTA curve, are attributed to thermal degradation and oxidation of QUE, respectively (Borghetti *et al.*, 2012; Costa *et al.*, 2002). The endothermic event at 310 °C in the DTA curve is associated with the melting followed by decomposition (Δm= 3.08%), as already reported in the literature (Borghetti *et al.*, 2012; Costa *et al.*, 2002).
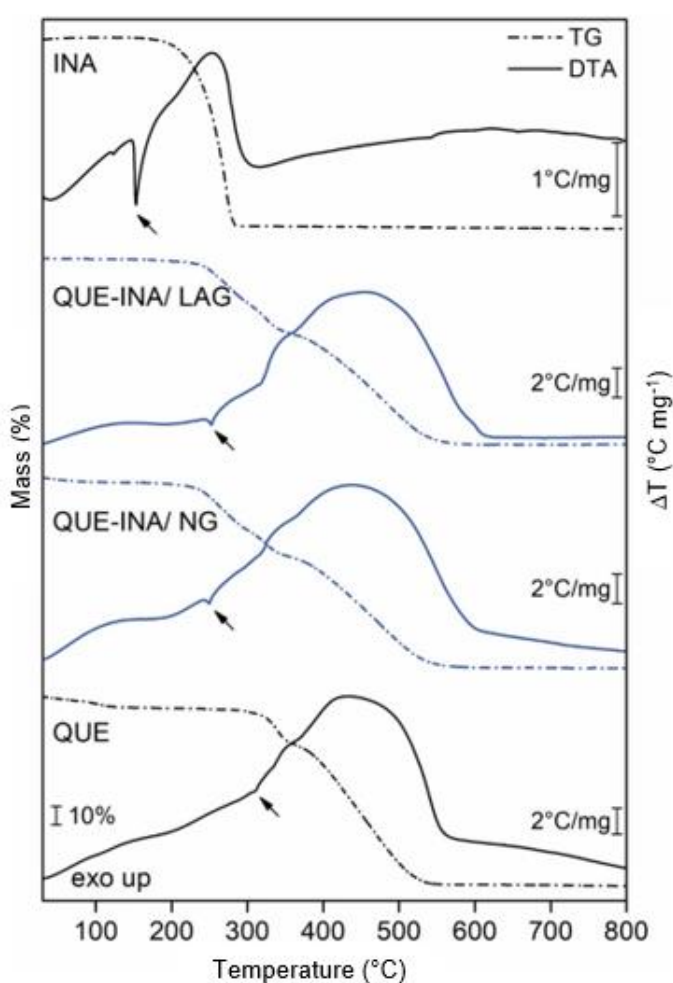

Figure 3. Simultaneous thermogravimetry-differential thermal analysis curves of QUE, INA, and the QUE–INA (1:1) systems (arrow: melting endothermic event).

The TG curve of INA shows a loss of mass in a single step between 175 and 285 °C, attributed to the evaporation of the compound. The two endothermic peaks at 123 and 153 °C in the DTA curve, without loss of mass on the TG curve, are associated with a phase transition (form II to form I) and the melting of the compound, respectively (Holanda *et al.*, 2019).

The thermoanalytical curves of the QUE–INA/NG and QUE–INA/LAG systems are similar, suggesting that the synthesis condition used does not significantly influence the formation of the multicomponent system, as already evidenced in the FTIR and XRPD data. These thermoanalytical curves show that the systems are thermally stable up to approximately 220 °C and undergo thermal decomposition in at least three overlapping mass loss steps, corresponding to endothermic and exothermic events in the DTA curve. The first step of mass loss, corresponding to an endotherm in the DTA curve, is attributed to the thermal decomposition of the QUE–INA system with the release of the INA coformer. The last two steps, corresponding to exothermic events in the DTA curve, are attributed to the thermal degradation of the remaining drug. The small endothermic peak at 252 °C in the DTA curve, already with a small mass loss in the TG curve, is attributed to the melting of the QUE–INA cocrystal, which has not yet undergone thermal degradation.

The thermal behavior presented by QUE–INA systems is quite different from that observed for isolated precursor compounds, which confirms the formation of the multicomponent solid form, according to the FTIR and XRPD results.

3.2 Quercetin–picolinamide (1:1) system

3.2.1 X-ray powder diffraction and FTIR

The XRPD diffractograms and FTIR spectra of the QUE, PA, and QUE–PA systems are shown in Fig. 4a and b, respectively.

The diffractograms of the QUE–PA/NG and QUE–PA/LAG systems present new diffraction peaks in 2θ equal to 5.1, 15.1, 20.1, 22.9, 25.7 and 36.7° and absence of peaks in 2θ equal to 5.5, 10.7, 14.1 and 17.9° (QUE) and 20.7 and 25.4° (PA), not being the combination of the diffractograms of its isolated precursors, which confirms the formation of the cocrystal. Furthermore, these results suggest that the addition of liquid in the mechanochemical synthesis does not significantly influence the formation of the new crystalline phase.

The FTIR spectrum of PA shows the spectral pattern reported for polymorph II of this compound (Akalin and Akyuz, 2006), which is the commonly marketed crystalline form. The main bands are observed at

$3416 \ \mathrm{cm^{-1}}$ attributed to asymmetric NH_2 stretching vibrations ($\nu_{asym}NH_2$), two bands at 3275 and $3170 \ \mathrm{cm^{-1}}$ attributed to symmetric NH_2 stretching vibrations ($\nu_{sym}NH_2$), a band at $1660 \ \mathrm{cm^{-1}}$ attributed to C=O stretching vibrations ($\nu C{=}O_{amide}$), a band at $1603 \ \mathrm{cm^{-1}}$ attributed to NH_2 bending (scissoring) vibrations (δNH_2 scissoring) and a band at $1391 \ \mathrm{cm^{-1}}$ attributed to C–N stretching vibrations of the amide group ($\nu C{-}N_{amide}$) (Akalin and Akyuz, 2006; Évora *et al.*, 2012).
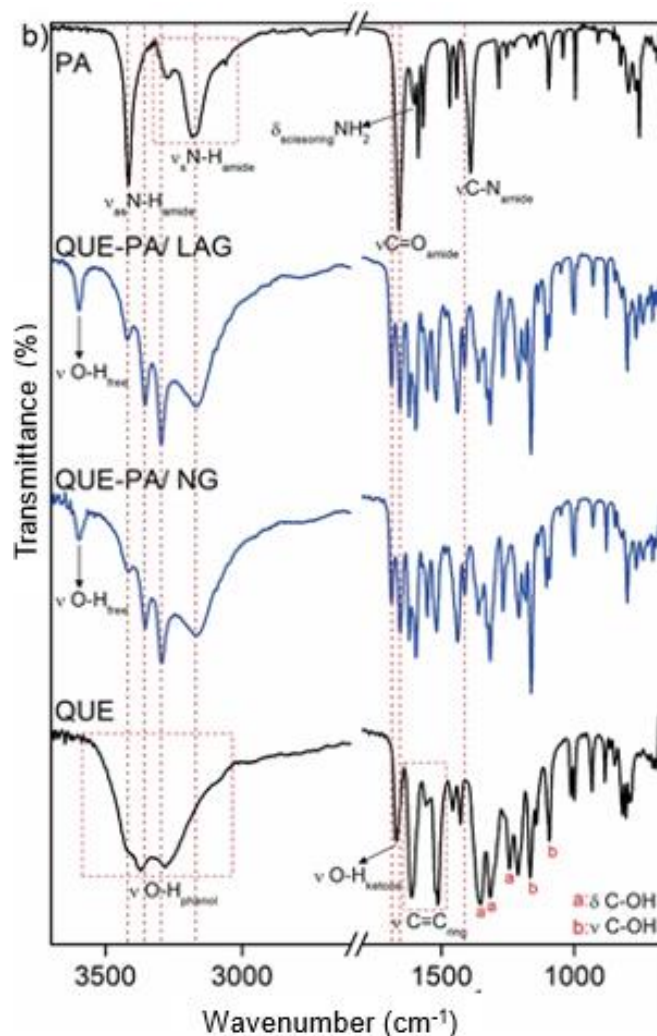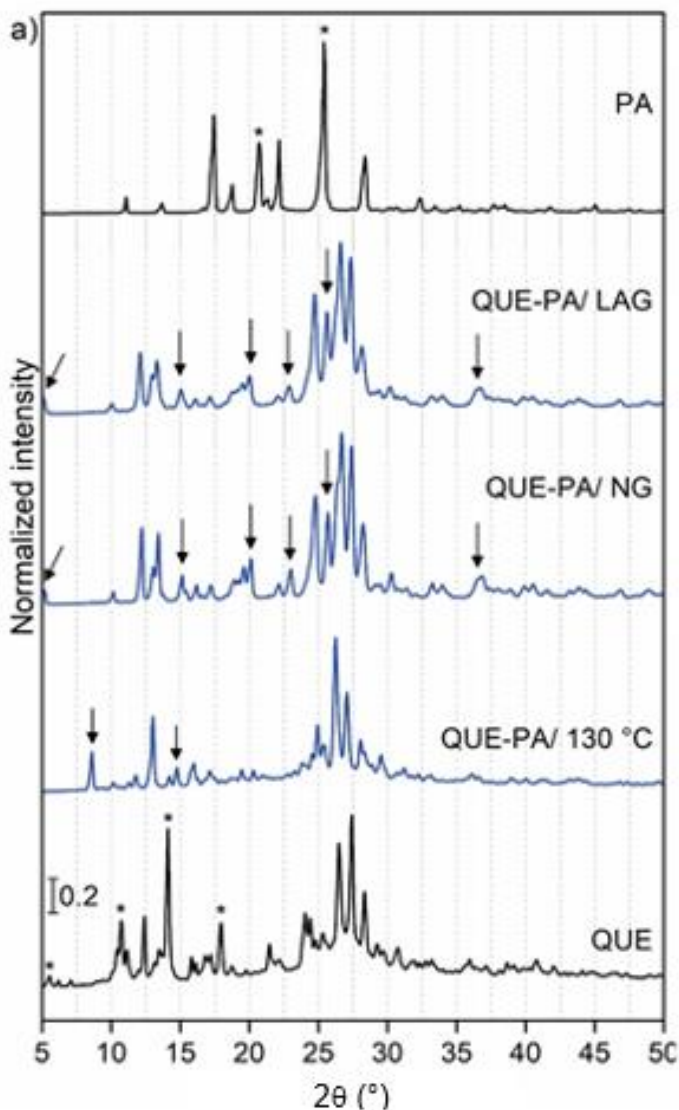

Figure 4. X-ray powder diffraction diffractograms **(a)** and FTIR spectra **(b)** of QUE, PA, and the QUE–PA (1:1) system**s**.

For the FTIR spectrum of the QUE–PA cocrystal, only small shifts in the bands associated with the functional groups of the precursors are observed, quite differently from the pronounced changes observed in the FTIR spectrum of the QUE–INA cocrystal. These results suggest that the supramolecular synthons established in the QUE–PA cocrystal are different from those present in the QUE–INA cocrystal, mainly due to the absence of changes in the spectra associated with the formation of the $OH_{(phenol)}{\cdots}N_{(aromatic)}$ synthon, probably the ortho position of the aromatic nitrogen in the PA molecule prevents the formation of this intermolecular interaction. This is also supported by the appearance of a weak band at $3599 \ \mathrm{cm^{-1}}$ attributed to O–H stretching vibrations of the free hydroxyl group ($\nu O{-}H$).

3.2.2 Simultaneous thermogravimetry-differential thermal analysis

The TG–DTA curves of QUE, PA, and QUE–PA systems are shown in Fig. 5. The TG curve of PA shows loss of mass in a single step between 130 and 235 °C, associated with a significant change in the baseline in the DTA curve, attributed to the vaporization of the compound. The endothermic peak at 105 °C in the DTA curve, without loss of mass in the TG curve, is attributed to the melting of the compound.
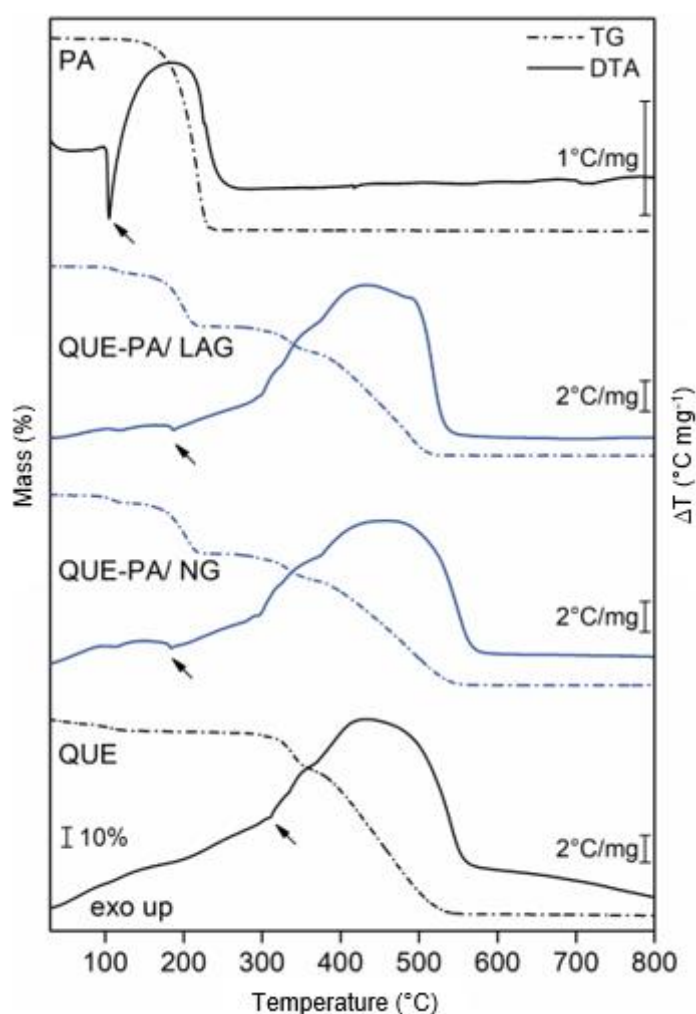

Figure 5. Simultaneous thermogravimetry-differential thermal analysis curves of QUE, PA, and the QUE–PA (1:1) systems (arrow: melting endothermic event).

The TG-DTA curves of the QUE–PA/NG and QUE–PA/LAG systems are very similar, suggesting that the condition of synthesis employed does not significantly influence the formation of the cocrystal, as already evidenced in the FTIR and XRPD data. These thermoanalytical curves show four steps of mass loss, corresponding to endothermic and exothermic events in the DTA curve. The first step, between 104 and 125 °C ($\Delta m_{QUE-PA/NG} = 4.02\%$; $\Delta m_{QUE-PA/LAG} = 3.16\%$), corresponding to a small endothermic event around 117 °C in the DTA curves, is attributed to the loss of a hydroxyl group ($\Delta m_{calc.} = 4.01\%$), probably free hydroxyl group, as indicated by the FTIR data. The XRPD diffractogram obtained from the sample heated to 130 °C, temperature above the first mass loss step, shows a new diffraction pattern, with a significant reduction in the number of diffraction peaks associated with cocrystal formation, decreased intensity, and displacement of other peaks and the appearance of two new peaks ($2\theta = 8.6$ and $14.8°$), suggesting that mass loss is associated with thermal degradation of the systems, as indicated by the calculated mass loss value.

After this first step, the remaining material is thermally stable up to 155 °C and undergoes thermal decomposition in three steps, between 155 and 525 °C. The second step, between 155 and 217 °C, is attributed to the thermal decomposition of the intermediate formed in the previous step with the release of PA ($\Delta m_{TG} = 28.12\%$; $\Delta m_{Calc.} = 28.77\%$). The last two steps, between 281 and 525 °C, are associated with thermal degradation of the remaining degraded QUE. The endothermic peak at 185 °C in the DTA curve, with a slight loss of mass in the TG curve, is attributed to the melting of the material. The thermal behavior presented by QUE–PA systems is quite different from that observed for isolated compounds, which confirms the formation of a cocrystal, according to the FTIR and XRPD results.

3.3 Quercetin–pyrazinoic acid (1:1) system

3.3.1 X-ray powder diffraction and FTIR

The XRPD diffractograms and FTIR spectra of the QUE–PZCA systems (Fig. 6) are just a combination of the diffractograms and spectra of the precursors, since no new diffraction peaks and band shifts are observed, suggesting that these systems are simple physical mixtures or eutectic mixtures.
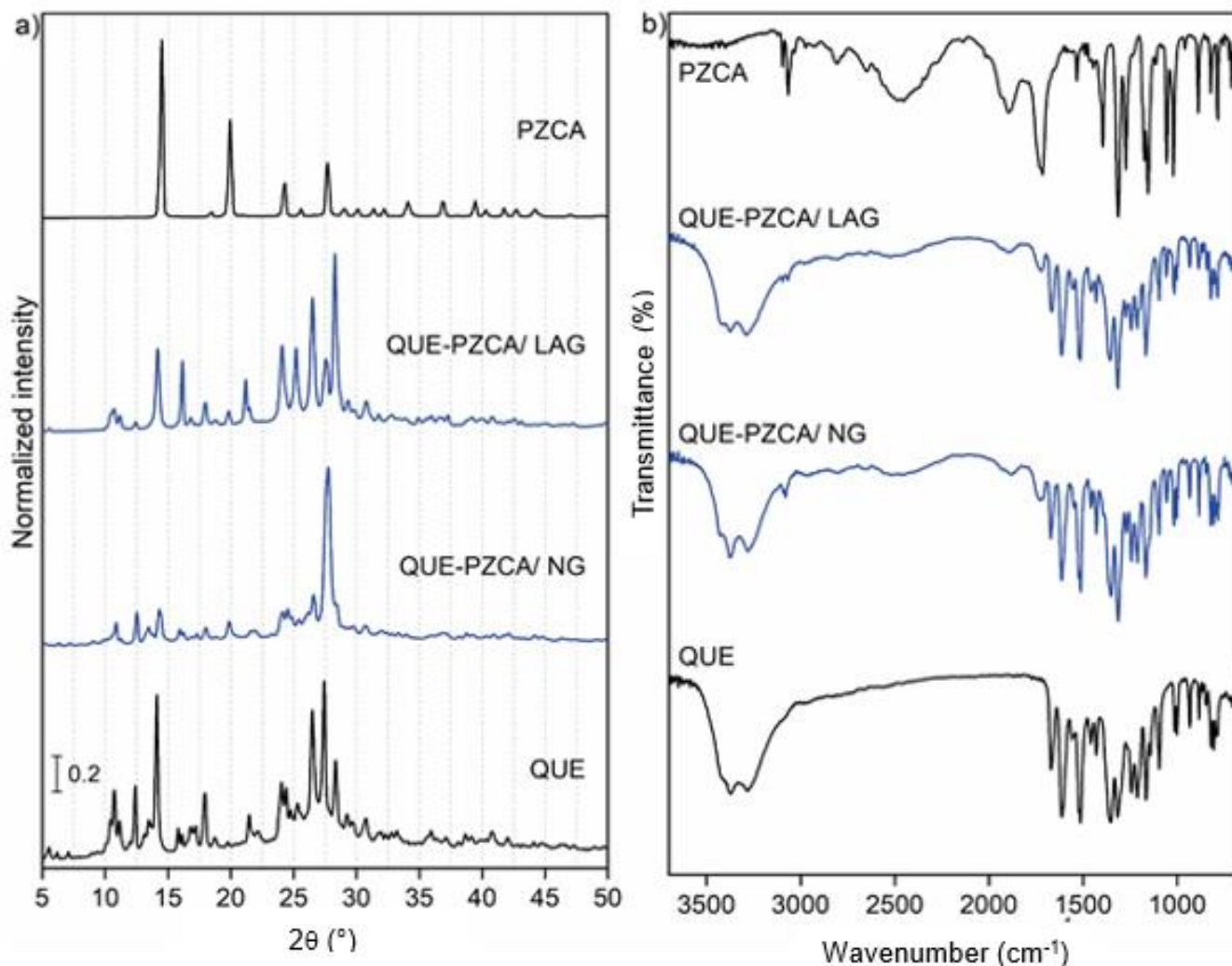
Figure 6. X-ray powder diffraction diffractograms (**a**) and FTIR spectra (**b**) of QUE, PZCA, and the QUE–PZCA (1:1) systems.

3.3.2 Simultaneous thermogravimetry-differential thermal analysis

The TG–DTA curves of the QUE, PZCA and the systems QUE–PZCA are shown in Fig. 7.

The TG–DTA curves of the PZCA show loss of mass in a single step between 160 and 229 °C, corresponding to partial sublimation and vaporization of the compound. The endothermic peak at 223 °C in the DTA curve is attributed to the melting of the compound (Almeida *et al.*, 2020).

The TG-DTA curves of the QUE–PZCA/LAG and QUE–PZCA/NG systems have similar thermal stability and the same three steps of mass loss. The first step, corresponding to a small endothermic peak at 207 °C in the DTA curve, is attributed to the sublimation and vaporization of PZCA. The second and third steps, associated with endothermic and exothermic events in the DTA curve, respectively, are associated with the

thermal degradation of QUE. In addition, the thermal profile and mass loss temperatures observed in the TG-DTA curves of the QUE–PZCA systems are similar to those observed in the TG-DTA curves of the isolated precursors, being the combination of the thermoanalytical curves of the isolated precursors. On the other hand, the thermal melting events of the precursors are not observed in the DTA curves of the systems, which may be related to the sensitivity of the DTA measurement and the lower amount of compound present in the QUE–PZCA systems.

The observed thermal behavior, together with the FTIR and XRPD data, confirm that QUE–PZCA systems are just simple physical mixtures.
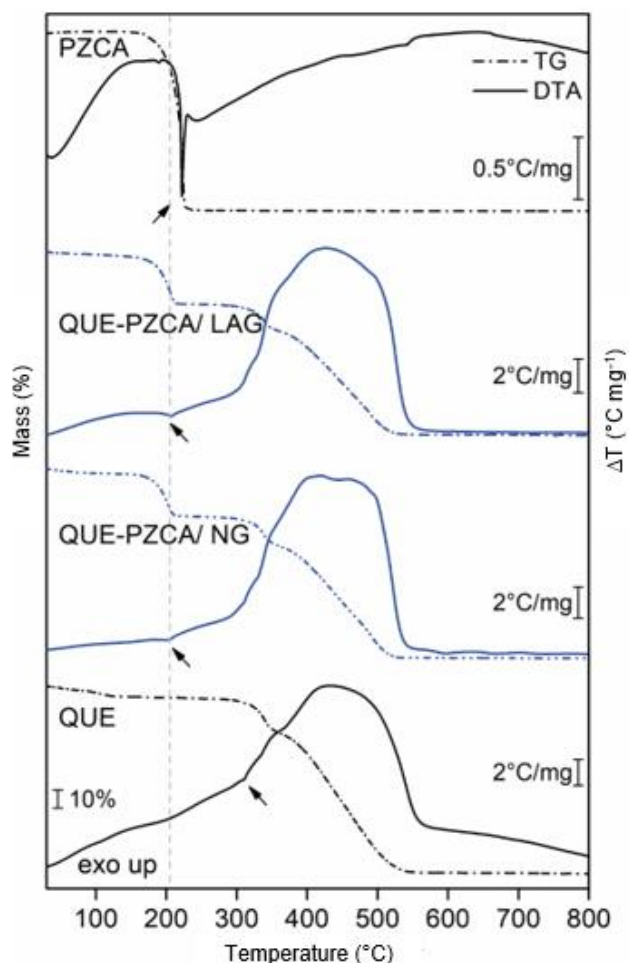
Figure 7. Simultaneous thermogravimetry-differential thermal analysis curves of QUE, PZCA, and the QUE–PZCA (1:1) systems.

3.4 Quercetin–benzamide (1:1) system

3.4.1 X-ray powder diffraction and FTIR

The XRPD diffractograms and FTIR spectra of the QUE–BA systems and their precursors are shown in Fig. 8.

As can be seen, both systems have similar diffraction and spectral patterns, corresponding to the combination of diffractograms and spectra of the starting materials, since no new diffraction peaks and band shifts are observed. This suggests that no new crystalline phases were formed, nor supramolecular synthons were established, which indicates that these systems are simple physical mixtures or eutectic mixtures.
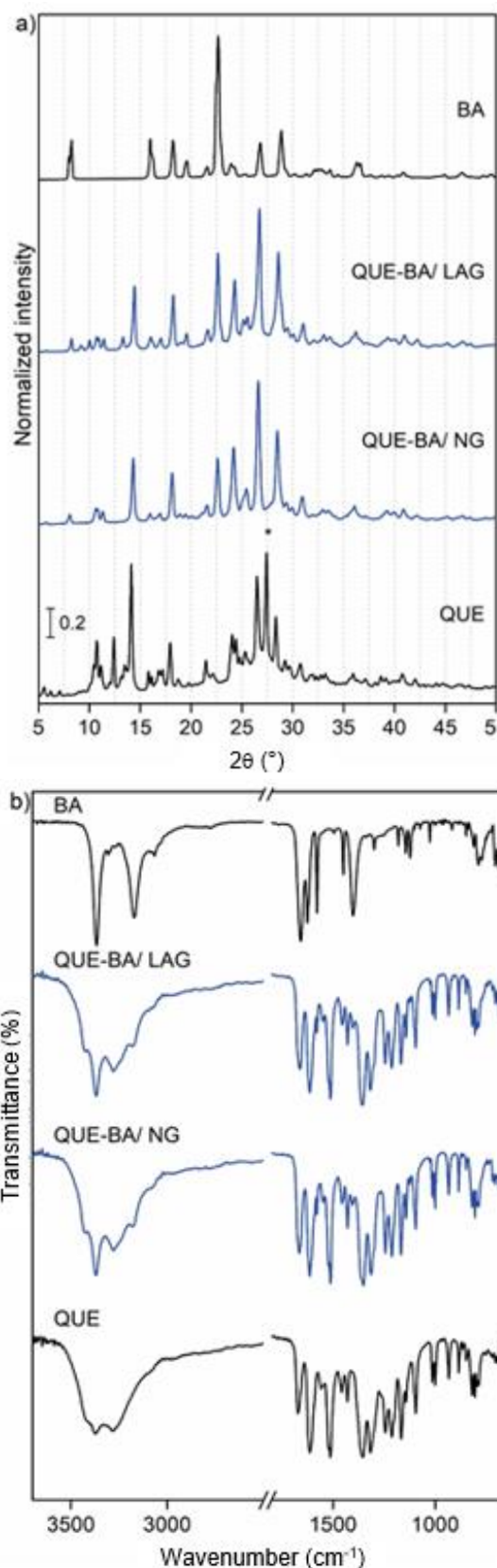

Figure 8. X-ray powder diffraction diffractograms **(a)** and FTIR spectra **(b)** of QUE, BA, and the QUE–BA (1:1) systems.

3.4.2 Simultaneous thermogravimetry-differential thermal analysis

The TG-DTA curves of the QUE, BA and the systems QUE–BA are shown in Fig. 9.

The TG-DTA curves of benzamide show mass loss in a single step between 155 and 255 °C, corresponding to a subtle endothermic event at 196 °C in the DTA curve, associated with the vaporization of the compound. The DTA curve shows an endothermic peak at 128 °C associated with the melting of the compound (Perpétuo *et al.*, 2014).

The TG curves of the QUE–BA systems show three stages of mass loss, corresponding to endothermic and exothermic events in the DTA curve. The first stage, between 150 and 230 °C, is attributed to the vaporization of BA. The last two steps, corresponding to endo and exothermic events in the DTA curve, are attributed to the thermal degradation of QUE. Furthermore, the DTA curves of both systems present two endothermic peaks at 115 and 305 °C, attributed to the melting of the precursors. The thermal behavior of this system is similar to that observed in the TG-DTA curves of the isolated compounds, suggesting that it is only the combination of the thermoanalytical curves. These thermoanalytical results, along with XRPD and FTIR data, suggest that the systems are just physical mixtures.

4. Conclusions

Although all coformers studied in this work have functional groups capable of forming supramolecular synthons with QUE, it was only possible to obtain cocrystals through the mechanochemical method with INA and PA isomers.

The FTIR data suggest that the supramolecular synthons formed in the QUE–INA and QUE–PA cocrystals are different, mainly regarding the presence of the $OH_{(phenol)} \cdots N_{(aromatic\ ring)}$ synthon present in the QUE–INA cocrystal, as already determined by data of crystalline structure and absent in the QUE-PA cocrystal. This is also suggested by the thermoanalytical data, since the thermal stability of the QUE–PA cocrystal is lower than that of the QUE–INA cocrystal, being associated with the loss of free hydroxyl groups (not participating in hydrogen bonds) present in the QUE–PA system.

In addition, the QUE–INA cocrystal, previously reported by the slurry method, could be obtained through a greener method.
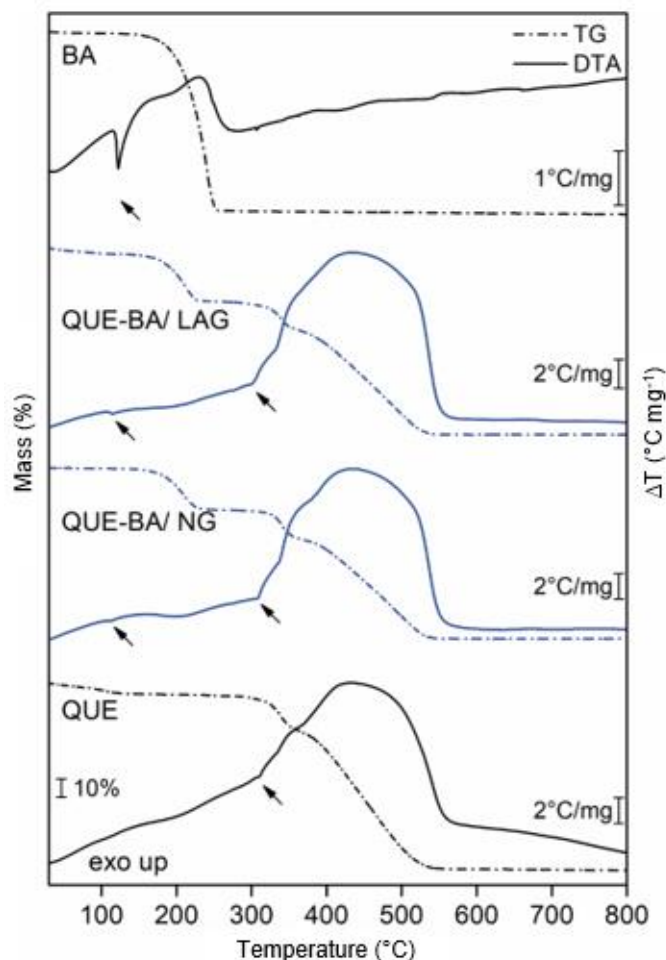

Figure 9. Simultaneous thermogravimetry-differential thermal analysis curves of QUE, BA, and the QUE–BA (1:1) systems (arrow: melting endothermic event).

Authors' contribution

Conceptualization: Souza, F. Z. R.; Almeida, A. C.; Caires, F. J.
Data curation: Souza, F. Z. R.; Almeida, A. C.
Formal Analysis: Souza, F. Z. R.
Funding acquisition: Caires, F. J.
Investigation: Souza, F. Z. R.; Almeida, A. C.; Ferreira, P. O.; Fernandes, R. P.
Methodology: Not applicable
Project administration: Caires, F. J.
Resources: Caires, F. J.
Software: Not applicable
Supervision: Caires, F. J.
Validation: Almeida, A. C.; Ferreira, P. O.
Visualization: Souza, F. Z. R.; Almeida, A. C.; Ferreira, P. O.; Caires, F. J.
Writing – original draft: Souza, F. Z. R.; Almeida, A. C.

References

Aakeröy, C.B.; Forbes, S.; Desper, J. Using Cocrystals To Systematically Modulate Aqueous Solubility and Melting Behavior of an Anticancer Drug. *J. Am. Chem. Soc.* **2009**, *131* (47), 17048–17049. https://doi.org/10.1021/ja907674c

Akalin, E.; Akyuz, S. Vibrational analysis of free and hydrogen bonded complexes of nicotinamide and picolinamide. *Vib. Spectrosc.* **2006**, *42* (2), 333–340. https://doi.org/10.1016/j.vibspec.2006.05.015

Almeida, A. C. de; Ferreira, P. O.; Torquetti, C.; Ekawa, B.; Carvalho, A. C. S.; Santos, E. C. dos; Caires, F. J. Mechanochemical synthesis, characterization and thermal study of new cocrystals of ciprofloxacin with pyrazinoic acid and p-aminobenzoic acid. *J. Therm. Anal. Calorim.* **2020**, *140* (5), 2293–2303. https://doi.org/10.1007/s10973-019-08958-3

Borghetti, G. S.; Carini, J. P.; Honorato, S. B.; Ayala, A. P.; Moreira, J. C. F.; Bassani, V. L. Physicochemical properties and thermal stability of quercetin hydrates in the solid state. *Thermochim. Acta*. **2012**, *539*, 109–114. https://doi.org/10.1016/j.tca.2012.04.015

Costa, E. M. da; Barbosa Filho, J. M.; Nascimento, T. G. do; Macêdo, R. O. Thermal characterization of the quercetin and rutin flavonoids. *Thermochim. Acta*. **2002**, *392–393*, 79–84. https://doi.org/10.1016/S0040-6031(02)00087-4

Dubey, R.; Desiraju, G. R. Combinatorial selection of molecular conformations and supramolecular synthons in quercetin cocrystal landscapes: a route to ternary solids. *IUCrJ*. **2015**, *2*(Part 4), 402–408. https://doi.org/10.1107/S2052252515009884

Évora, A. O. L.; Castro, R. A. E.; Maria, T. M. R.; Rosado, M. T. S.; Silva, M. R.; Canotilho, J.; Eusébio, M. E. S. Resolved structures of two picolinamide polymorphs. Investigation of the dimorphic system behaviour under conditions relevant to co-crystal synthesis. *CrystEngComm*. **2012**, *14* (24), 8649–8657. https://doi.org/10.1039/c2ce26244d

Friščić, T.; Childs, S. L.; Rizvi, S. A. A.; Jones, W. The role of solvent in mechanochemical and sonochemical cocrystal formation: a solubility-based approach for predicting cocrystallisation outcome. *CrystEngComm*. **2009**, *11* (3), 418–426. https://doi.org/10.1039/B815174A

Holanda, B. B. C.; Alarcon, R. T.; Gaglieri, C.; Souza, A. R. de; Castro, R. A. E.; Rosa, P. C. P.; Tangerino, D. J. A.; Bannach, G. Thermal studies, degradation kinetic, equilibrium solubility, DFT, MIR, and XRPD analyses of a new cocrystal of gemfibrozil and isonicotinamide. *J. Therm. Anal. Calorim.* **2019**, *136* (5), 2049–2062. https://doi.org/10.1007/s10973-018-7873-8

Karagianni, A.; Malamatari, M.; Kachrimanis, K. Pharmaceutical Cocrystals: New Solid Phase Modification Approaches for the Formulation of APIs. *Pharmaceutics*. **2018**, *10* (1), 18. https://doi.org/10.3390/pharmaceutics10010018

Karimi-Jafari, M.; Padrela, L.; Walker, G. M.; Croker, D. M. Creating Cocrystals: A Review of Pharmaceutical Cocrystal Preparation Routes and Applications. *Cryst. Growth Des.* **2018**, *18* (10), 6370–6387. https://doi.org/10.1021/acs.cgd.8b00933

Kavanagh, O. N.; Croker, D. M.; Walker, G. M.; Zaworotko, M. J. Pharmaceutical cocrystals: from serendipity to design to application. *Drug Discov. Today*. **2019**, *24* (3), 796–804. https://doi.org/10.1016/j.drudis.2018.11.023

Madaan, K.; Lather, V.; Pandita, D. Evaluation of polyamidoamine dendrimers as potential carriers for quercetin, a versatile flavonoid. *Drug Deliv.* **2016**, *23* (1), 254–262. https://doi.org/10.3109/10717544.2014.910564

Nguyen, T. T.; Jeong, J.-H. Development of a single-jet electrospray method for producing quercetin-loaded poly (lactic-co-glycolic acid) microspheres with prolonged-

release patterns. *J. Drug Deliv. Sci. Technol*. **2018**, *47*, 268–274. https://doi.org/10.1016/j.jddst.2018.07.005

Panzade, P.; Shendarkar, G.; Shaikh, S.; Rathi, P. B. Pharmaceutical Cocrystal of Piroxicam: Design, Formulation and Evaluation. *Adv. Pharm. Bull*. **2017**, *7* (3), 399–408. https://doi.org/10.15171/apb.2017.048

Patel, R. D.; Raval, M. K.; Bagathariya, A. A.; Sheth, N. R. Functionality improvement of Nimesulide by eutectic formation with nicotinamide: Exploration using temperature-composition phase diagram. *Adv. Powder Technol*. **2019**, *30* (5), 961–973. https://doi.org/10.1016/j.apt.2019.02.010

Perpétuo, G. L.; Gálico, D. A.; Guerra, R. B.; Moreira, R.; Chierice, G. O.; Bannach, G. Thermal, spectroscopic and DFT studies of solid benzamide. *Braz. J. Therm. Anal.* **2014**, *3* (1–2), 5–10. https://doi.org/10.18362/bjta.v3i1-2.23

Qiao, N.; Li, M.; Schlindwein, W.; Malek, N.; Davies, A.; Trappitt, G. Pharmaceutical cocrystals: An overview. *Int. J. Pharm.* **2011**, *419* (1–2), 1–11. https://doi.org/10.1016/j.ijpharm.2011.07.037

Rajput, L.; Sanphui, P.; Desiraju, G. R. New Solid Forms of the Anti-HIV Drug Etravirine: Salts, Cocrystals, and Solubility. *Cryst. Growth Des*. **2013**, *13* (8), 3681–3690. https://doi.org/10.1021/cg4007058

Ramešová, Š.; Sokolová, R.; Degano, I.; Bulíčková, J.; Žabka, J.; Gál, M. On the stability of the bioactive flavonoids quercetin and luteolin under oxygen-free conditions. *Anal. Bioanal. Chem*. **2012**, *402* (2), 975–982. https://doi.org/10.1007/s00216-011-5504-3

Rautenberg, M.; Bhattacharya, B.; Akhmetova, I.; Emmerling, F. Mechanochemical and solution syntheses of two novel cocrystals of orcinol with two N,N′-Dipyridines: Structural diversity with varying ligand flexibility. *J. Mol. Struct*. **2020**, *1217*, 128303. https://doi.org/10.1016/j.molstruc.2020.128303

Ravikumar, N.; Gaddamanugu, G.; Solomon, K. A. Structural, spectroscopic (FT-IR, FT-Raman) and theoretical studies of the 1:1 cocrystal of isoniazid with p-coumaric acid. *J. Mol. Struct*. **2013**, *1033*, 272–279. https://doi.org/10.1016/j.molstruc.2012.10.029

Refat, M. S.; Hamza, R. Z.; Adam, A. M. A.; Saad, H. A.; Gobouri, A. A.; Al-Harbi, F. S.; Al-Salmi, F. A.; Altalhi, T.; El-Megharbel, S. M. Quercetin/Zinc complex and stem cells: A new drug therapy to ameliorate glycometabolic control and pulmonary dysfunction in diabetes mellitus: Structural characterization and genetic studies. *PLoS One*. **2021**, *16* (3), e0246265. https://doi.org/10.1371/journal.pone.0246265

Sathisaran, I.; Dalvi, S. V. Engineering Cocrystals of Poorly Water-Soluble Drugs to Enhance Dissolution in Aqueous Medium. *Pharmaceutics*. **2018**, *10* (3), 108. https://doi.org/10.3390/pharmaceutics10030108

Sinha, A. S.; Maguire, A. R.; Lawrence, S. E. Cocrystallization of Nutraceuticals. *Cryst. Growth Des*. **2015**, *15* (2), 984–1009. https://doi.org/10.1021/cg501009c

Smith, A. J.; Kavuru, P.; Wojtas, L.; Zaworotko, M. J.; Shytle, R. D. Cocrystals of Quercetin with Improved Solubility and Oral Bioavailability. *Mol. Pharm*. **2011**, *8* (5), 1867-1876. https://doi.org/10.1021/mp200209j

Su, H.; He, H.; Tian, Y.; Zhao, N.; Sun, F.; Zhang, X.; Jiang, Q.; Zhu, G. Syntheses and characterizations of two curcumin-based cocrystals. *Inorg. Chem. Commun.* **2015**, *55*, 92–95. https://doi.org/10.1016/j.inoche.2015.03.027

Tang, Y.; Nakashima, S.; Saiki, S.; Myoi, Y.; Abe, N.; Kuwazuru, S.; Zhu, B.; Ashida, H.; Murata, Y.; Nakamura, Y. 3,4-Dihydroxyphenylacetic acid is a predominant biologically-active catabolite of quercetin glycosides. *Food Res. Int*. **2016**, *89* (1), 716–723. https://doi.org/10.1016/j.foodres.2016.09.034

Thakuria, R.; Sarma, B. Drug-Drug and Drug-Nutraceutical Cocrystal/Salt as Alternative Medicine for Combination Therapy: A Crystal Engineering Approach. *Crystals*. **2018**, *8* (2), 101. https://doi.org/10.3390/cryst8020101

Varzakas, T.; Zakynthinos, G.; Verpoort, F. Plant Food Residues as a Source of Nutraceuticals and Functional Foods. *Foods*. **2016**, *5* (4), 88. https://doi.org/10.3390/foods5040088

Vasisht, K.; Chadha, K.; Karan, M.; Bhalla, Y.; Jena, A.K.; Chadha, R. Enhancing biopharmaceutical parameters of bioflavonoid quercetin by cocrystallization. *CrystEngComm*. **2016**, *18* (8), 1403–1415. https://doi.org/10.1039/C5CE01899D

Yadav, A. V.; Shete, A. S.; Dabke, A. P.; Kulkarni, P. V.; Sakhare, S.S. Co-crystals: A novel approach to modify physicochemical properties of active pharmaceutical ingredients. *Indian J. Pharm. Sci*. **2009**, *71* (4), 359–370. https://doi.org/10.4103/0250-474X.57283

Yousef, M.A.E.; Vangala, V.R. Pharmaceutical Cocrystals: Molecules, Crystals, Formulations, Medicines. *Cryst. Growth Des*. **2019**, *19* (12), 7420–7438. https://doi.org/10.1021/acs.cgd.8b01898

Yurdakul, Ş.; Ataç, A. Fourier Transform-Infrared Spectroscopic Study of IsonicotinamideMetal(II) Tetracyanonickelate and Halide Complexes. *Spectrosc. Lett.* **2004**, *37* (1), 33–42. https://doi.org/10.1081/SL-120028421